

The Scale for the Expansion of the Universe: From Local Structures to Cosmology

David Benisty^{1,*}

¹*Leibniz-Institut für Astrophysik Potsdam, An der Sternwarte 16, D-14482 Potsdam, Germany*

This study tackles the impact dark energy in different systems by a simple unifying formalism. We introduce a parameter space to compare gravity tests across all cosmic scales, using the McVittie spacetime (MCV), that connect spherically symmetric solutions with cosmological solutions. By analyzing invariant scalars, the Ricci, Weyl, and Kretschmann scalars, we develop a phase-space description that predicts the dominance of the Cosmological Constant. We explore three cases: (1) the local Hubble flow around galaxy groups and clusters, (2) spherical density distributions and (3) binary motion. Our results show that galaxy groups and clusters exhibit Kretschmann scalar values consistent with the Cosmological Constant curvature, indicating where dark energy dominates.

Keywords: Dark Energy; Dark Matter; Local Universe; Galaxy Dynamics

I. INTRODUCTION

Dark Energy (DE) is one of the most enigmatic puzzles in contemporary cosmology. Introduced to account for the detected accelerated expansion of the cosmos, DE is hypothesized to be an unidentified energy type that pervades all of space, generating repulsive effects to offset gravitational pull on large cosmic scales [1]. Its identification, prompted by observations of Type Ia supernovae, revolutionized our comprehension of the universe's structure and evolutionary trajectory [2]. The concept of DE as the principal driver of cosmic acceleration has gained reinforcement from diverse observational data, such as measurements of the cosmic microwave background (CMB) and analyses of large-scale cosmic structures. Although DE is primarily examined in cosmological contexts, its impact also reaches smaller astrophysical environments, including galaxy clusters, particularly near transitional zones like the zero-velocity surface, where universal expansion shifts to localized gravitational collapse [3]. This interplay between local and global DE effects provides a unique opportunity to probe its properties across a wide range of scales.

This study examines DE phenomena across cosmological and local scales using the MCV spacetime as a theoretical model. The MCV metric characterizes a spherically symmetric mass embedded in an expanding universe, serving as a versatile tool to analyze DE's interplay between localized and cosmic regimes. By studying the spacetime's curvature features, we pinpoint areas where DE's effects dominate and assess their relevance for testing gravitational theories across different scales—from strong-field environments near dense objects to large-scale cosmological evolution, extending the work by [4]. This methodology bridges DE's influence on cosmic dynamics, connecting its behavior in compact astrophysical settings to its role in shaping the universe's large-scale structure.

This paper is organized as follows: Section II discuss the spacetime and its limiting cases. Section III discusses

the geodesic equation for the MCV spacetime. Section IV discusses the expansion domination in different regimes. Section V discusses the results.

II. GENERAL SPACETIME

A general framework for describing bound systems embedded in an expanding cosmological background is provided by the MCV metric [5, 6]. For a flat cosmological background, this metric takes the form:

$$ds^2 = - \left(1 - \Phi - \frac{r^2 H^2}{c^2} \right) c^2 dt^2 - \frac{2rH}{\sqrt{1-\Phi}} dt, c, dr + \frac{dr^2}{1-\Phi} + r^2 d\Omega^2, \quad (1)$$

where $\Phi \equiv 2GM/rc^2$ represents the gravitational potential, $H \equiv \dot{a}/a$ is the Hubble parameter and Ω is the angular part of the metric. Here, M is the total mass of the structure, G is the Newtonian gravitational constant, and c is the speed of light. The metric reduces to the Friedmann-Lemaître-Robertson-Walker (FLRW) metric in the absence of a local mass ($\Phi = 0$ and $M = 0$), and to the Schwarzschild metric when the Hubble parameter vanishes ($H = 0$), corresponding to a static, isolated mass. In the special case where $H = \text{Const}$ and $\Phi = 0$, the metric simplifies to the de Sitter metric, describing a universe dominated by a cosmological constant. In Eq. (1), r represents the physical spatial coordinate, which is related to the comoving coordinate by $\chi = r/a(t)$. By setting $M = 0$ and using the comoving coordinate, we recover the standard flat FLRW metric, which describes a homogeneous and isotropic universe:

$$ds^2 = -(c^2 - r^2 H^2) dt^2 - 2rH dt dr + dr^2 + r^2 d\Omega^2 = -c^2 dt^2 + a^2 (d\chi^2 + \chi^2 d\Omega^2). \quad (2)$$

Similarly, setting $H = 0$ reduces the metric to the Schwarzschild metric. See [7] for a further discussion.

To analyze the curvature properties of the MCV spacetime, we compute three key curvature scalars: the Ricci scalar \mathcal{R} , the Weyl scalar \mathcal{C} , and the Kretschmann scalar

* benidav@aip.de

\mathcal{K} . These scalars provide a comprehensive description of the spacetime's geometry, capturing the interplay between local gravitational effects and cosmic expansion. The Ricci scalar \mathcal{R} reflects the overall curvature influenced by both the local mass and the cosmological expansion. The Weyl scalar \mathcal{C} characterizes the tidal forces generated by the local mass, which dominate near compact objects. The Kretschmann scalar \mathcal{K} combines contributions from both local and global curvature, offering a complete measure of the spacetime's curvature invariants:

$$\begin{aligned} \mathcal{R} &= \frac{12H^2}{c^2} \left(1 - \frac{3}{4} \frac{1+w}{\sqrt{1-\Phi}} \right), \quad \mathcal{C} = 12 \left(\frac{\Phi}{r^2} \right)^2, \\ \mathcal{K} &= \frac{12\Phi^2}{r^4} + \frac{24H^4}{c^4} \left(1 - \frac{3}{2} \frac{1+w}{\sqrt{1-\Phi}} + \frac{9}{8} \frac{(1+w)^2}{1-\Phi} \right), \end{aligned} \quad (3)$$

where $w \equiv -1 - 2\dot{H}/3H^2$ is the equation of state of the background universe. For a dark energy-dominated universe, $w = -1$; for a matter-dominated universe, $w = 0$; and for a radiation-dominated era, $w = 1/3$. To quantify the relative strength of local gravitational effects compared to cosmic expansion, we introduce the following dimensionless parameters:

$$\begin{aligned} D_H &\equiv \frac{c}{H}, \quad r_s = \frac{2GM}{c^2} = r\Phi, \\ \kappa &\equiv \frac{\Phi}{r^2} \frac{2H^2}{c^2} = \frac{GM}{H^2 r^3}, \quad \tau \equiv \frac{1+w}{\sqrt{1-\Phi}}. \end{aligned} \quad (4)$$

Using these parameters, the curvature scalars can be expressed as:

$$\begin{aligned} \mathcal{R} &= \frac{12}{D_H^2} \left(1 - \frac{3}{4}\tau \right), \quad \mathcal{C} = 12 \frac{r_s^2}{r^6}, \\ \mathcal{K} &= 48 \frac{r_s^2}{r^6} + \frac{24}{D_H^4} \left(1 - \frac{3}{2}\tau + \frac{9}{8}\tau^2 \right). \end{aligned} \quad (5)$$

The MCV metric enables the investigation of how bound systems, such as galaxies or galaxy clusters, evolve within an expanding cosmological background. The dimensionless parameter κ determines the ratio between these two parts and as we will see from different systems has different interpretation.

III. TEST PARTICLE GEODESIC

To describe binary motion in the presence of dark energy, we consider the low-energy limit of the geodesic equation over the metric (1), which gives:

$$\ddot{r} = -\frac{GM}{r^2} + \frac{\ddot{a}}{a}r = -\frac{GM}{r^2} - \frac{(1+3w)}{2}H^2r. \quad (6)$$

The first term represents the Newtonian gravitational attraction, while the second term accounts for the influence of dark energy, which acts as a repulsive force proportional to the Hubble parameter.

We can solve the motion analytically only for the Newtonian case, with the eccentricity parameter e and the phase parameter η . These solutions describe the evolution of the radial coordinate r , the radial velocity v_r , and the tangential velocity v_t as functions of time t . For bounded systems, where $e \in [0, 1]$ the radial coordinate r and time t are given by [8, 9]:

$$\begin{aligned} r &= \frac{r_{\text{ta}}}{2} (1 - e \cos \eta), \quad t = \frac{t_{\text{ta}}}{\pi} (\eta - e \sin \eta), \\ v_r &= \frac{\pi r_{\text{ta}}}{2 t_{\text{ta}}} \frac{e \sin \eta}{1 - e \cos \eta}, \quad v_t = \frac{\pi r_{\text{ta}}}{2 t_{\text{ta}}} \frac{\sqrt{1-e^2}}{1 - e \cos \eta}, \end{aligned} \quad (7)$$

where r_{ta} and t_{ta} are the turnaround radius and turnaround time, respectively, with $e \in [1, \infty]$. For the unbounded dwarf galaxies, the radial coordinate r and time t are expressed as:

$$\begin{aligned} r &= \frac{r_{\text{ta}}}{2} (e \cosh \eta - 1), \quad t = \frac{t_{\text{ta}}}{\pi} (e \sinh \eta - \eta), \\ v_r &= \frac{\pi r_{\text{ta}}}{2 t_{\text{ta}}} \frac{e \sinh \eta}{e \cosh \eta - 1}, \quad v_t = \frac{\pi r_{\text{ta}}}{2 t_{\text{ta}}} \frac{\sqrt{1-e^2}}{e \cosh \eta - 1}. \end{aligned} \quad (8)$$

The enclosed mass is given by: $M = \pi^2 r_{\text{ta}}^3 / 8Gt_{\text{ta}}^2$. Since any test particle has its own r_{ta} and t_{ta} , we use the common age of the Universe t_U and the common central mass of the object M to express the distance and velocities with respect to e and η :

$$\begin{aligned} r &= r_0 \frac{1 - e \cos \eta}{(\eta - e \sin \eta)^{2/3}}, \quad v_r = \frac{r_0}{t_U} e \sin \eta \frac{(\eta - e \sin \eta)^{1/3}}{1 - e \cos \eta}, \\ r &= r_0 \frac{e \cosh \eta - 1}{(e \sinh \eta - \eta)^{2/3}}, \quad v_r = \frac{r_0}{t_U} e \sinh \eta \frac{(e \sinh \eta - \eta)^{1/3}}{e \cosh \eta - 1}. \end{aligned} \quad (9)$$

where r_0 is related to the mass via: $r_0^3 = GMt_U^2$.

The solutions for different values of e and η are illustrated in Fig. 1, which shows the velocity-distance relation for both bounded and unbounded systems and the interplay between the gravity and the local expansion of groups.

IV. EXPANSION DOMINATION

To evaluate the DE's dominance, specific criteria are utilized. These parameters identify the regimes where dark energy's repulsive influence overcomes gravitational attraction, governing the evolution of cosmic systems.

A. Hubble Flow around Galaxy Groups and Clusters

The Hubble flow describes the motion of galaxies due to the expansion of the universe. On smaller scales, such as within galaxy groups or clusters, gravitational interactions cause deviations from this uniform expansion. [8] introduced a method to estimate the mass of a system

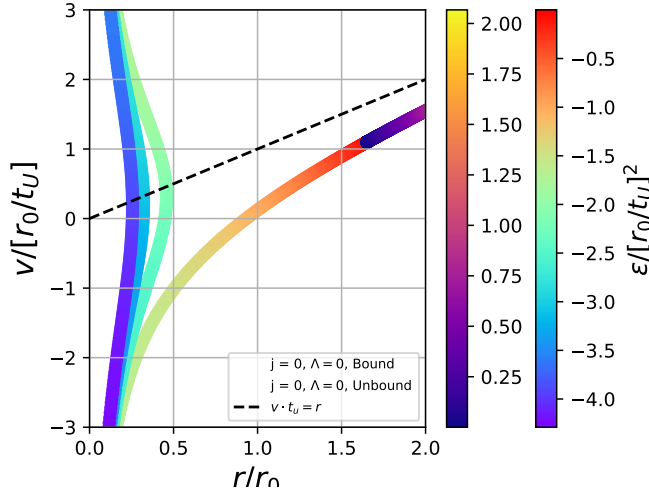


FIG. 1. The normalized velocity-distance relation from the analytical solution (9). The solution is scaled with r_0 and r_0/t_U , where t_U is the age of the Universe. The turnaround r_0 is related to the enclosed mass. The colored lines corresponds to $e = 1$. For different e the area between the colored lines is also covered. The dashed line marks the asymptotic behavior for the unbound solution (which in the case of $H \neq 0$ corresponds to the Hubble flow).

using the Hubble Flow. It is possible to jointly constrain the mass of the bound structure and H_0 from an observed velocity-distance diagram. This approach has been applied to galaxy groups in [10–14], and to galaxy clusters in [15, 16]. Beyond the spherical case, the domination of DE can be determined by the turnaround of galaxy groups and clusters, as discussed in [3, 17–19]. For a discussion how to connect the line-of-sight velocities into the radial velocities, see Ref. [20–22].

Fig. 2 shows an isolated halo from the IllustrisTNG simulations [23] with a mass of $\sim 10^{12} M_\odot$. The upper panel illustrates the bounded and unbounded subhalos around the turnaround. Refs. [24, 25] use different semi-analytical solutions for the local interplay with the Hubble flow, which take the form:

$$v(r) = \alpha H_0 r - \beta \sqrt{\frac{GM}{r}}, \quad (10)$$

with $\alpha = 1.3$ and $\beta = 1.1$. The red line in the figure shows the corresponding fit for the interplay branch. For comparison, we consider observational data on dwarf galaxies in the local environment, taken from [26–29]¹. The lower panel of Fig. 2 shows the radial velocity versus distance from the center of mass of the Local Group (LG). The bounded area, which includes the Milky Way, M31, and their dwarf galaxies, shows a spread up to the turnaround

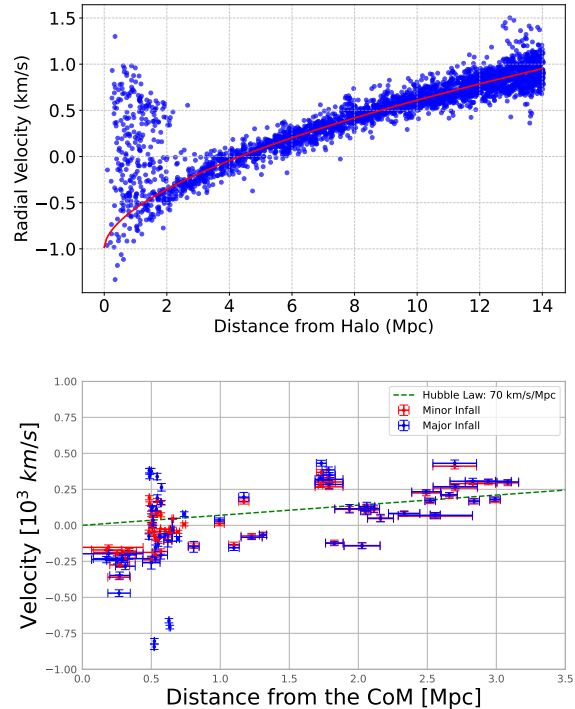


FIG. 2. **Upper:** The velocity vs. distance for an isolated halo from the IllustrisTNG simulation. **Lower:** The radial velocity of galaxies as a function of their distance from the halo CoM. A green dashed line illustrates the theoretical Hubble Law with a slope of 70 km/s/Mpc, representing the expected outward velocity for galaxies due to the universe’s expansion.

radius. Beyond this, we observe the local interplay to the Hubble expansion.

Asymptotically, the \ddot{a}/a term in Eq. (6) approaches $-\frac{(1+3w)}{2}H^2 = \Omega_\Lambda H_0^2$, which is the value for a de-Sitter universe. The maximal turnaround, with the condition $\ddot{r} = 0$, leads to:

$$r_{\text{ta}} \leq r_\Lambda \equiv \sqrt[3]{\frac{GM}{\Omega_\Lambda H_0^2}}. \quad (11)$$

This distance represents the maximal limit for a test particle within this potential. Ref. [3] discusses systems and their turnaround radii, showing that for bounded galaxy groups and clusters, this is the maximal turnaround. For instance, the LG has a maximal turnaround of 1.5 Mpc (from Eq. (11) with $M = 3 \cdot 10^{12} M_\odot$), while [24, 25] report $r_{\text{ta}} \approx 1$ Mpc.

The curvature scalar \mathcal{K} and dimensionless parameter κ for galaxy groups and clusters are written as:

$$\mathcal{K} = \mathcal{C}(1 + 2\kappa), \quad \kappa = \left(\frac{r}{r_\Lambda}\right)^3. \quad (12)$$

In the context of curvature scalars, the maximal turnaround modifies the Kretschmann scalar to: $[\mathcal{K}]_{\text{ta}} =$

¹ LG and Nearby Dwarf Galaxies Link

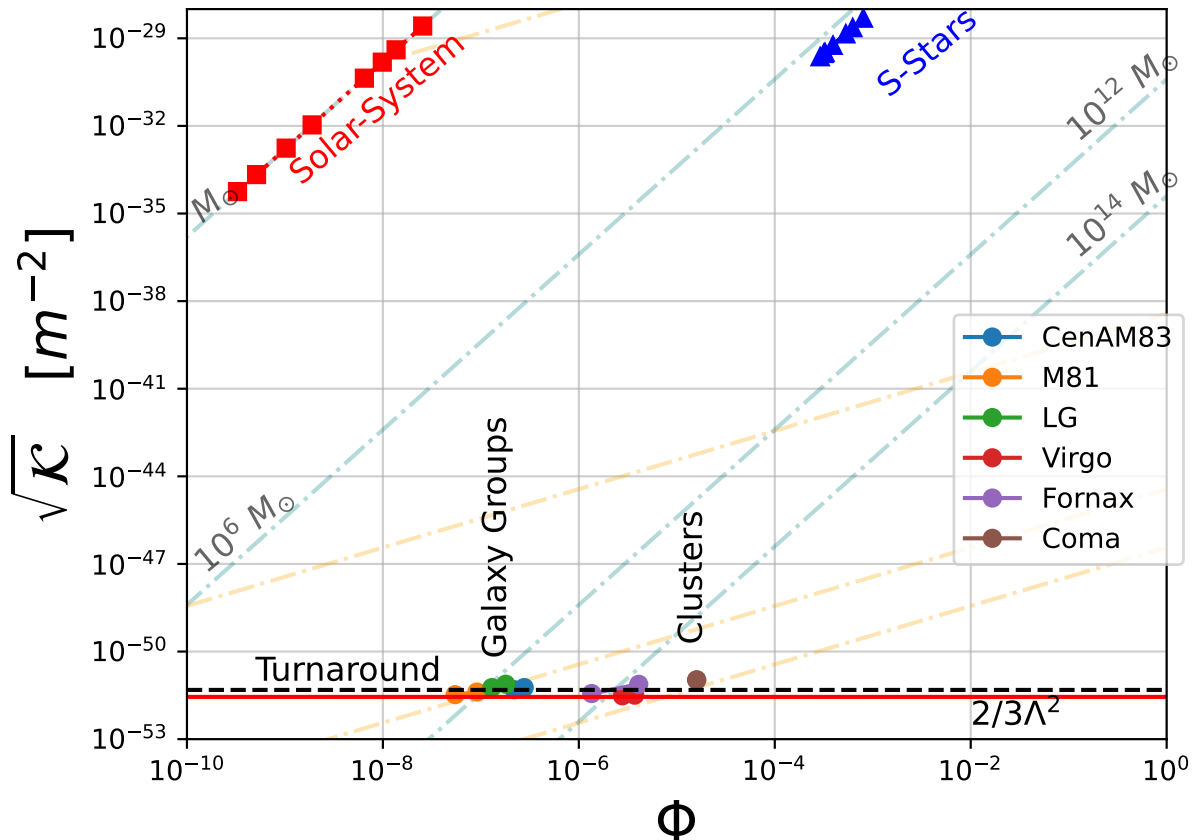


FIG. 3. The curvature phase space for the potential Φ versus the scalar $\sqrt{\kappa}$ in a de-Sitter $w = -1$ universe. The Solar System and S-stars around the galactic center are positioned much higher than galaxy groups and clusters, which lie at the transition to local expansion, indicating the dominance of Λ in larger structures.

$3[\mathcal{K}]_{\text{Cos}}$, where the cosmological Kretschmann scalar is $[\mathcal{K}]_{\text{Cos}} \equiv 12/D_H^2$. Here, spacetime curvature is dominated by the background expansion, as the contribution from concentrated mass becomes negligible. If the curvature nears the cosmological value, the expansion dominates motion, as seen for dwarf galaxies outside the turnaround. For the bounded region, the Kretschmann scalar is much higher and Newtonian-dominated, indicating negligible Λ effects.

To study the dynamics of galaxy groups and clusters, we analyze systems such as the CenA/M83, LG, M81 groups, and the Virgo, Fornax, and Coma clusters [29, 30]. We employ their turnaround radii and total enclosed masses to compute curvature parameters. Galaxy groups typically have masses of approximately $\sim 10^{12} M_\odot$ or greater, while clusters reside in the $\sim 10^{14} M_\odot$ or higher mass range. As illustrated in Fig. 3, all analyzed systems align with the $[\mathcal{K}]_{\text{ta}}$ line, demonstrating that dwarf galaxies near the turnaround radius exist at a transition zone between large-scale cosmic expansion and localized gravitational collapse.

B. Spherical Density

The curvature scalar for spherical density ρ_m in an expanding ρ_Λ reads:

$$\mathcal{R} = \frac{32\pi G\rho_\Lambda}{c^2}, \quad \mathcal{C} = \frac{256\pi^2 G^2 \rho_m}{c^4}, \quad \mathcal{K} = \mathcal{C}(1 + \Delta_c) \quad (13)$$

where parameter κ (from Eq. 4) changes into Δ_c is the ratio between the densities: $\Delta_c \equiv \rho_m/\rho_\Lambda$, with $\rho_\Lambda = 8\pi G/\Lambda c^2$. The parameter emerges in the Kretschmann scalar and quantifies the interplay between the local density of the object and the global cosmological density, that highlights the connection between local gravitational effects and the large-scale influence of dark energy.

This transition is formalized in the Spherical Collapse Model [31, 32], which outlines the growth of a small initial density perturbation. The overdensity gradually detaches from the Hubble flow, expands to a maximum turnaround radius and begins to collapse. Collisionless dynamics arrest the collapse, leading to virialization at a final radius which is half of the turnaround radius. The critical overdensity Δ_c quantifies the contrast between the virialized density and the background density at col-

lapse time in a matter-dominated universe. This yields:

$$\Delta_c \approx 18\pi^2 \approx 178, \quad (14)$$

implying virialized halos are approximately 178 times denser than their cosmological surroundings or $\Delta_c \approx 200$. Λ CDM cosmology predicts marginally smaller values owing to dark energy's influence [33].

C. Binary Motion

In the context of binary motion [34, 35], the curvature scalars for binary systems can be expressed as:

$$\mathcal{C} = \frac{12\omega_{\text{kep}}^2}{c^4}, \quad \mathcal{K} = \frac{12\omega_{\text{kep}}^2 + 24H^4}{c^4} = \mathcal{C}(1 + 2\kappa), \quad (15)$$

where ω_{kep} is the Keplerian orbital frequency. The ratio κ naturally emerges from \mathcal{K} , highlighting the interplay between orbital dynamics and dark energy:

$$\kappa = \left(\frac{T_{\text{Kep}}}{T_H} \right)^2, \quad (16)$$

where $T_{\text{Kep}} = 2\pi\sqrt{r^3/GM}$ is the Keplerian orbital period, and $T_H \equiv 2\pi/H_0 \approx 27.6$ Gyr is the Hubble time, calculated from the measured Planck values [36]. To probe the effect of Λ , one must identify systems with orbital periods close to T_H . Notably, T_H is much larger than the age of the Universe (~ 13.7 Gyr), indicating that dark energy's influence on binary systems is subtle and becomes significant only over cosmological timescales.

The LG has the longest orbital period among bounded binary systems discussed in this paper. Since the orbital period of the LG is about $\approx 0.62T_H$, the upper bound on Λ is expected to be tighter than those derived from the solar system or the S2 star. Ref. [35] finds the upper bound on Λ to be 5 times larger than the Planck value [37]. Ref. [35] shows that two main characteristics determine the effect of Λ : the accuracy of the measurements and the period of the system. Although the solar system provides more accurate measurements than the LG, the upper limit on Λ derived from the solar system is about 10^{-46} m^{-2} , which is approximately 10 orders of magnitude larger than the actual value. In contrast, the LG's longer orbital period results in a tighter upper limit, demonstrating the importance of system timescales in constraining dark energy.

V. CURVATURE PHASE SPACE AND DISCUSSION

This research explores the dominance of DE across various astrophysical systems by analyzing curvature

scalars. We unify the description of gravitational effects from small-scale systems, such as the Solar System, to large-scale structures like galaxy clusters, using the MCV spacetime as a theoretical framework. By examining the interplay between local gravitational dynamics and cosmological expansion, we identify regions where DE dominates using the scalar invariant from General Relativity.

For spherically symmetric objects, binary motion, and dwarf galaxies orbiting main halos, dimensionless parameters quantify the ratio between the curvature arising from mass attraction and the curvature arising from the expansion of the universe. These parameters include the spherical density Δ_c , which represents the ratio between the enclosed matter density and the cosmological density; the binary system parameter κ , defined as the ratio of the orbital period squared to the Hubble parameter squared; and the galaxy group and cluster parameter κ , which is the ratio of the turnaround radius to the distance determined by Λ . These dimensionless constants emerge naturally in the curvature scalars and characterize the interplay between local gravitational attraction and the expansion of the universe.

The curvature scalars serve as key indicators of this transition, emerging naturally from fundamental theory and providing a unified framework for understanding the influence of dark energy. Fig. (3) illustrates the curvature phase space for the potential Φ versus the scalar $\sqrt{\mathcal{K}}$ in a de-Sitter universe. The Solar System and S-stars are positioned much higher in the phase space, reflecting strong local gravitational effects, while galaxy groups and clusters lie at the transition to local expansion, where DE dominates. This contrast highlights the scale-dependent influence of dark energy: smaller systems remain dominated by local gravity, whereas larger structures exhibit curvature scalars that approach their cosmological values, indicating the dominance of DE. By comparing systems of varying sizes, we have shown that DE dominates in larger structures, such as galaxy groups and clusters, where the curvature scalars align with cosmological predictions. This phase-space analysis provides a clear and unified framework for understanding the interplay between local gravitational dynamics and the large-scale expansion of the universe driven by dark energy.

The cases studied in this research are based on idealized cases. To probe the changes in galaxy groups and cluster with more complicated environment, we use N-body simulations. In that way, the upper panel of Fig (2) shows that the theoretical model fit to the simulation.

ACKNOWLEDGMENTS

DB thanks Salvatore Capozziello and Jenny Wagner for useful discussions and suggestions. DB is supported by a Minerva Fellowship of the Minerva Stiftung Gesellschaft fuer die Forschung mbH.

-
- [1] P. J. E. Peebles and B. Ratra, *Rev. Mod. Phys.* **75**, 559 (2003), [arXiv:astro-ph/0207347 \[astro-ph\]](#).
- [2] S. Perlmutter *et al.* (Supernova Cosmology Project), *Astrophys. J.* **517**, 565 (1999), [arXiv:astro-ph/9812133 \[astro-ph\]](#).
- [3] V. Pavlidou, N. Tetradis, and T. N. Tomaras, *JCAP* **05**, 017 (2014), [arXiv:1401.3742 \[astro-ph.CO\]](#).
- [4] T. Baker, D. Psaltis, and C. Skordis, *Astrophys. J.* **802**, 63 (2015), [arXiv:1412.3455 \[astro-ph.CO\]](#).
- [5] G. C. McVittie, *Mon. Not. Roy. Astron. Soc.* **93**, 325 (1933).
- [6] R. Nandra, A. N. Lasenby, and M. P. Hobson, *Mon. Not. Roy. Astron. Soc.* **422**, 2931 (2012), [arXiv:1104.4447 \[gr-qc\]](#).
- [7] I. Antoniou and L. Perivolaropoulos, *Phys. Rev. D* **93**, 123520 (2016), [arXiv:1603.02569 \[gr-qc\]](#).
- [8] A. Sandage, *Astrophys. J.* **307**, 1 (1986).
- [9] I. D. Karachentsev, O. G. Kashibadze, D. I. Makarov, and R. B. Tully, *Mon. Not. Roy. Astron. Soc.* **393**, 1265 (2009), [arXiv:0811.4610 \[astro-ph\]](#).
- [10] S. Peirani and J. A. de Freitas Pacheco, *New Astron.* **11**, 325 (2006), [arXiv:astro-ph/0508614 \[astro-ph\]](#).
- [11] S. Peirani and J. A. de Freitas Pacheco, *Astron. Astrophys.* **488**, 845 (2008), [arXiv:0806.4245 \[astro-ph\]](#).
- [12] J. Peñarrubia, Y.-Z. Ma, M. G. Walker, and A. McConnachie, *Mon. Not. R. Astron. Soc.* **443**, 2204 (2014), [arXiv:1405.0306 \[astro-ph.GA\]](#).
- [13] J. G. Sorce, S. Gottlöber, Y. Hoffman, and G. Yepes, *Mon. Not. R. Astron. Soc.* **460**, 2015 (2016), [arXiv:1605.06756 \[astro-ph.CO\]](#).
- [14] A. Del Popolo and M. H. Chan, *Astrophys. J.* **926**, 156 (2022), [arXiv:2210.10397 \[astro-ph.CO\]](#).
- [15] Y. J. Kim, J. Kang, M. G. Lee, and I. S. Jang, *Astrophys. J.* **905**, 104 (2020), [arXiv:2010.01364 \[astro-ph.CO\]](#).
- [16] O. G. Nasonova, J. A. de Freitas Pacheco, and I. D. Karachentsev, *Astron. Astrophys.* **532**, A104 (2011), [arXiv:1106.1291 \[astro-ph.CO\]](#).
- [17] Y. J. Kim, J. Kang, M. G. Lee, and I. S. Jang, *Astrophys. J.* **905**, 104 (2020), [arXiv:2010.01364 \[astro-ph.CO\]](#).
- [18] V. Pavlidou and T. N. Tomaras, *JCAP* **09**, 020 (2014), [arXiv:1310.1920 \[astro-ph.CO\]](#).
- [19] D. Tanoglidis, V. Pavlidou, and T. Tomaras, *JCAP* **12**, 060 (2015), [arXiv:1412.6671 \[astro-ph.CO\]](#).
- [20] I. D. Karachentsev and O. G. Kashibadze, *Astrophysics* **49**, 3 (2006).
- [21] I. D. Karachentsev and O. G. Nasonova, *Mon. Not. R. Astron. Soc.* **405**, 1075 (2010), [arXiv:1002.2085 \[astro-ph.CO\]](#).
- [22] J. Wagner and D. Benisty, (2025), [arXiv:2501.13149 \[astro-ph.GA\]](#).
- [23] D. Nelson *et al.*, *Comput. Astrophys. Cosmol.* **6**, 2 (2019), [arXiv:1812.05609 \[astro-ph.GA\]](#).
- [24] S. Peirani and J. A. de Freitas Pacheco, *New Astron.* **11**, 325 (2006), [arXiv:astro-ph/0508614](#).
- [25] J. Peñarrubia, Y.-Z. Ma, M. G. Walker, and A. McConnachie, *Mon. Not. Roy. Astron. Soc.* **443**, 2204 (2014), [arXiv:1405.0306 \[astro-ph.GA\]](#).
- [26] A. W. McConnachie, *Astron. J.* **144**, 4 (2012), [arXiv:1204.1562 \[astro-ph.CO\]](#).
- [27] A. W. McConnachie and K. A. Venn, *Astron. J.* **160**, 124 (2020), [arXiv:2007.05011 \[astro-ph.GA\]](#).
- [28] A. W. McConnachie and K. A. Venn, *Research Notes of the American Astronomical Society* **4**, 229 (2020), [arXiv:2012.03904 \[astro-ph.GA\]](#).
- [29] R. B. Tully *et al.*, *Astrophys. J.* **944**, 94 (2023), [arXiv:2209.11238 \[astro-ph.CO\]](#).
- [30] I. D. Karachentsev, D. I. Makarov, and E. I. Kaisina, *Astron. J.* **145**, 101 (2013), [arXiv:1303.5328 \[astro-ph.CO\]](#).
- [31] J. E. Gunn and J. R. Gott, III, *Astrophys. J.* **176**, 1 (1972).
- [32] P. J. E. Peebles, *The large-scale structure of the universe* (1980).
- [33] F. Pace, S. Meyer, and M. Bartelmann, *JCAP* **10**, 040 (2017), [arXiv:1708.02477 \[astro-ph.CO\]](#).
- [34] D. Benisty, A.-C. Davis, and N. W. Evans, *Astrophys. J. Lett.* **953**, L2 (2023), [arXiv:2306.14963 \[astro-ph.CO\]](#).
- [35] D. Benisty, J. Wagner, and D. Staicova, *Astron. Astrophys.* **683**, A83 (2024), [arXiv:2310.11488 \[astro-ph.CO\]](#).
- [36] N. Aghanim *et al.* (Planck), *Astron. Astrophys.* **641**, A6 (2020), [Erratum: *Astron. Astrophys.* 652, C4 (2021)], [arXiv:1807.06209 \[astro-ph.CO\]](#).
- [37] N. Aghanim *et al.* (Planck), *Astron. Astrophys.* **641**, A6 (2020), [Erratum: *Astron. Astrophys.* 652, C4 (2021)], [arXiv:1807.06209 \[astro-ph.CO\]](#).